The electronic supplementary information for

Enhancement of Visible Light Photocatalysis by Grafting ZnO Nanoplatelets with Exposed (0001) Facets onto a Hierarchical Substrate

Shan He,[a] Shitong Zhang,[a] Jun Lu,[a] Yufei Zhao,[a] Jing Ma,[b] Min Wei,[a,*] David G. Evans,[a] and Xue Duan[a]

[a] *State Key Laboratory of Chemical Resource Engineering, Beijing University of Chemical Technology, Beijing 100029, P. R. China*

[b] *School of Chemistry and Chemical Engineering, Key Laboratory of Mesoscopic Chemistry of MOE, Nanjing University, Nanjing 210093, P. R. China*

1. Experimental details

Preparation of amorphous Al_2O_3 microspheres: Amorphous Al_2O_3 microspheres were prepared by the hydrothermal method reported previously.[1] In a typical procedure, $Al_2(SO_4)_3 \cdot 18H_2O$ (0.007 mol), urea ($CO(NH_2)_2$) (0.028 mol) and sodium tartrate (0.025 mol) were dissolved in distilled water (70 mL) and then the solution was transferred into an autoclave, followed by hydrothermal treatment at 165 ºC for 2 h. The precipitate was separated by centrifugation, washed thoroughly with water and anhydrous alcohol, and dried at 100 °C for 3 h. Amorphous Al_2O_3 microspheres were obtained by calcination of the above precipitate at 500 ºC for 6 h.

Preparation of the F-LDH: The hierarchical F-LDH was prepared by an in situ growth technique similar to a previous report by our group.[2] $Zn(NO_3)_2 \cdot 6H_2O$ (0.01 mol) and NH_4NO_3 (0.06 mol) were dissolved in deionized water (100 mL), and 3% ammonia solution was then slowly added until the pH reached 6.5. The amorphous Al_2O_3 microspheres were placed in the above solution in

an autoclave at 80 °C for 48 h. Finally, the F-LDH was separated by centrifugation, rinsed with ethanol and dried at room temperature.

Preparation of the F-MMO: F-LDH was calcined in air at 500 °C for 6 h, with a heating rate of 2 °C/min. The calcination process results in the phase transformation of the F-LDH to F-MMO. The resulting product was slowly cooled to room temperature.

Preparation of the ZnAl-MMO powder sample: The ZnAl-LDH precursor (Zn/Al = 2.0) was synthesized by a hydrothermal method. A solution of $Zn(NO_3)_2 \cdot 6H_2O$ (1.2×10^{-1} M) and $Al(NO_3)_3 \cdot 9H_2O$ (6.0×10^{-2} M) in deionized water (200 mL) was added dropwise over 2 h to a solution of NaOH (3.1×10^{-1} M) and $NaNO_3$ (2.1×10^{-1} M) in water (100 mL). The mixture was heated at 343 K for 24 h. The precipitate was separated by centrifugation, washed thoroughly with water and dried at 343 K for 20 h. The ZnAl-MMO powder sample was obtained by calcination of ZnAl-LDH precursor in air at 500 °C for 6 h with a heating rate of 2 °C /min.

Preparation of the ZnO nanoplates and ZnO nanorods: These were prepared by the solvothermal methods reported previously.[3,4]

Photocatalytic reaction: The visible light photocatalytic activity of the F-MMO was evaluated by the photocatalytic decomposition of a model pollutant Rhodamine B (RhB). A 300 W Xe lamp (Beijing Perfectlight PLS-SXE300/300UV) was used as a light source with a cutoff filter to provide visible light irradiation (λ >400 nm). The experiments were performed at ambient temperature as follows: a 100 mg of F-MMO catalyst was added to a 40 mL of RhB solution (1.0×10^{-5} M). Before illumination, the suspension was stirred for 30 min in the dark to reach the adsorption–desorption equilibrium between RhB and the photocatalyst. Then the suspension was stirred and exposed to visible light irradiation, and the concentration of RhB was monitored by a UV-visible spectrophotometer during the photodegradation process. The procedure was performed

over 10 cycles to evaluate the performance catalyst when repeatedly used. The photocatalytic activities of ZnAl-MMO powder sample, ZnO nanoplates and ZnO nanorods were also evaluated in the same way.

Characterization: Powder X-ray diffraction (XRD) measurements were performed on a Rigaku XRD-6000 diffractometer, using Cu Kα radiation (λ = 0.15418 nm) at 40 kV, 30 mA, with a scanning rate of 10° min^{-1}, and a 2θ angle ranging from 3° to 70°. The morphology of the film samples was investigated using a Zeiss Supra 55 scanning electron microscope (SEM) with an accelerating voltage of 20 kV. Transmission electron microscopy (TEM) images were recorded with Philips TECNAI-20 and JEOL JEM-2010 high resolution transmission electron microscopes. The accelerating voltage was 200 kV. UV-vis absorption spectra were recorded on a Shimadzu UV-2501PC spectrometer equipped with an integrating sphere. Inductively coupled plasma—atomic emission spectroscopy (ICP–AES, Shimadzu ICPS-7500) was used to measure the content of Zn in the F-MMO sample. The specific surface area determination and pore size analysis were performed by the BET and BJH methods, respectively, using a Quantachrome Autosorb-1C-VP analyzer. Prior to the measurements, samples were degassed at 200 °C for 2 h.

2. Details of the DFT calculations

It is well-known that atoms near a surface adopt a rather different packing from those in the bulk state. For solid ZnO, surface atoms will undergo a so called geometry optimization process (i.e. relaxation) by which the atoms move to the lowest free energy state.[5] In this work, we computationally simulated such relaxation process on the $(10\bar{1}0)$, (0001) and $(000\bar{1})$ surfaces that were constructed by cleaving the wurtzite ZnO unit cell. A slab thickness of ~18 Å was used to obtain meaningful results; the vacuum width of 15 Å was used for surface relaxation (as shown in Scheme S3), which ensures that interactions between two neighboring slabs can be ignored.[6] The

bottom three atom-layers were frozen at their bulk positions during structural optimization, whereas the top layers were relaxed. The CASTEP program module in Materials Studio (MS) 4.0 software of Accelrys Inc. was employed to implement all the theoretical calculations in this study.[7] The generalized gradient approximation (GGA) with the Perdew–Burke–Ernzerhof (PBE) functional was employed for the DFT exchange correlation energy.[8,9] A 340 eV cutoff was assigned to the plane-wave basis set. The self-consistent field (SCF) tolerance was 1×10^{-6} eV. Ultrasoft pseudopotentials were used to describe the electron–ion interactions.[10] The electronic wavefunctions were obtained using a density-mixing scheme.

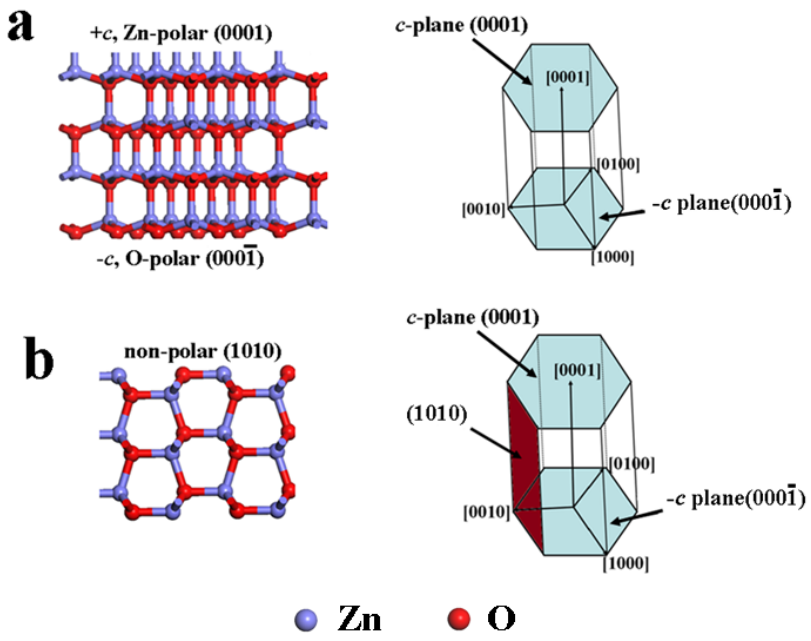

Scheme S1. Schematic representations of the hexagonal cell of ZnO displaying the main crystallographic planes and atomic arrangement for (a) Zn-polar (0001) and O-polar $(000\,\bar{1})$ facets along the *c*-axis with the corresponding polarization field; (b) the nonpolar $(10\,\bar{1}\,0)$ facet of ZnO.

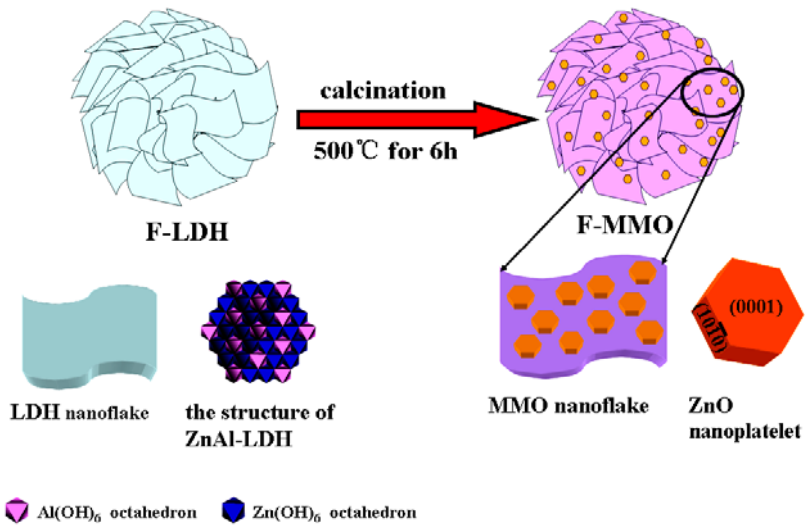

Scheme S2. Schematic illustration of the formation of ZnO nanoplatelets with a high degree of exposure of (0001) facets on the surface of the F-MMO substrate via the in situ topotactic transformation.

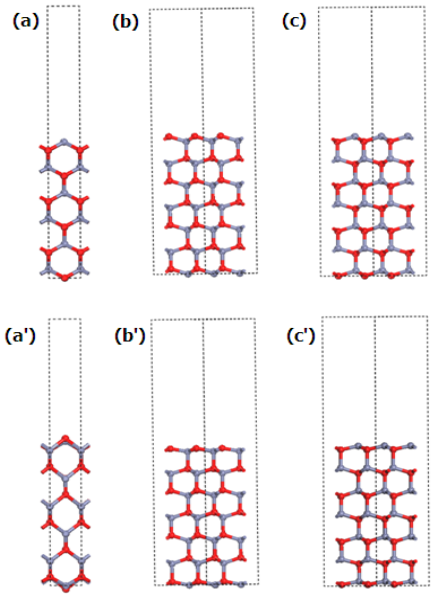

Scheme S3. Vacuum slab structures of the (a) unrelaxed (10 $\bar{1}$ 0) surface, (a´) relaxed (10 $\bar{1}$ 0)surface; (b) unrelaxed (0001) surface, (b´) relaxed (0001) surface; (c) unrelaxed (000 $\bar{1}$) surface, and (c´) relaxed (000 $\bar{1}$) surface.

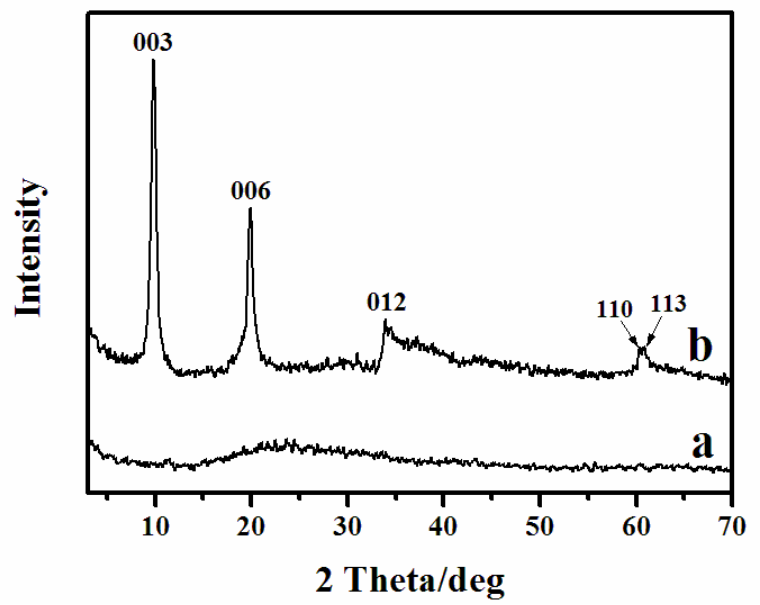

Fig. S1 XRD patterns of (a) the amorphous Al_2O_3 microspheres; (b) the as-prepared F-LDH crystallized at 80 °C for 48 h.

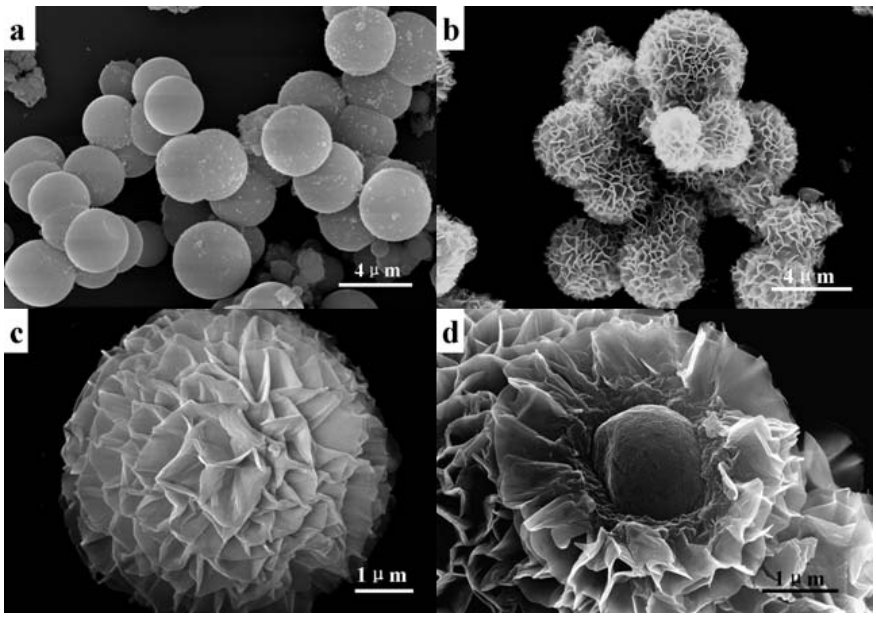

Fig. S2 (a) SEM image of the amorphous Al_2O_3 microspheres; SEM images of the as-prepared F-LDH at (b) low magnification and (c) high magnification; (d) SEM sectional image of a single microsphere exhibiting the structure of the LDH flowerlike shell/ the amorphous Al_2O_3 core.

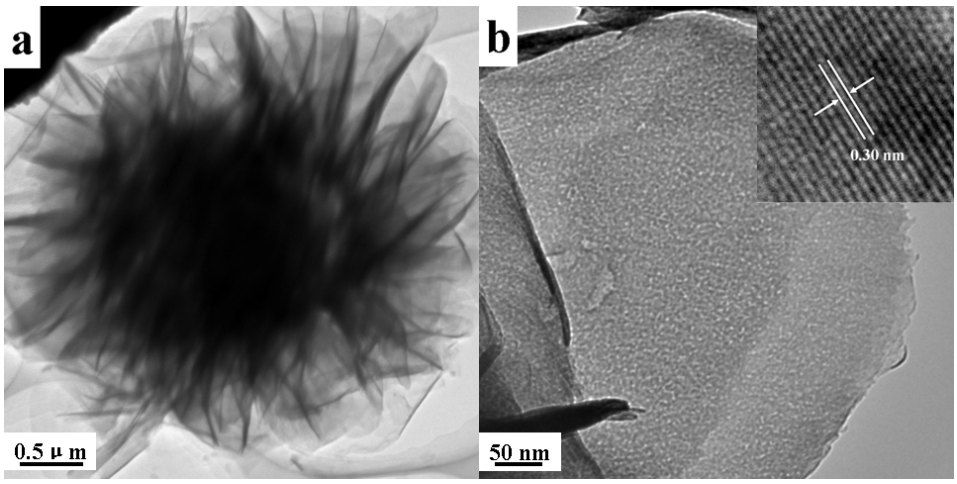

Fig. S3 (a) High-magnification TEM image of an individual F-LDH hierarchical microsphere; (b) TEM image of a single LDH nanoflake selected from (a). Inset: the corresponding HRTEM image of the LDH nanoflake.

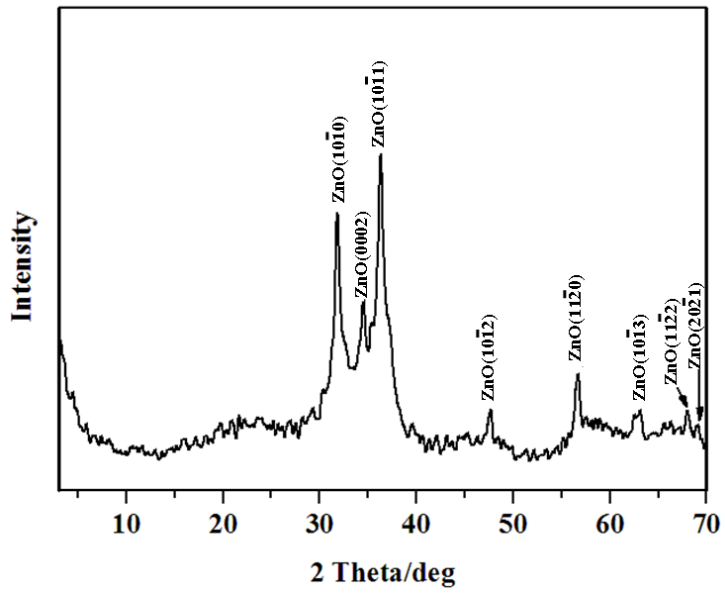

Fig. S4 XRD pattern of the F-MMO sample obtained by calcination of the F-LDH precursor.

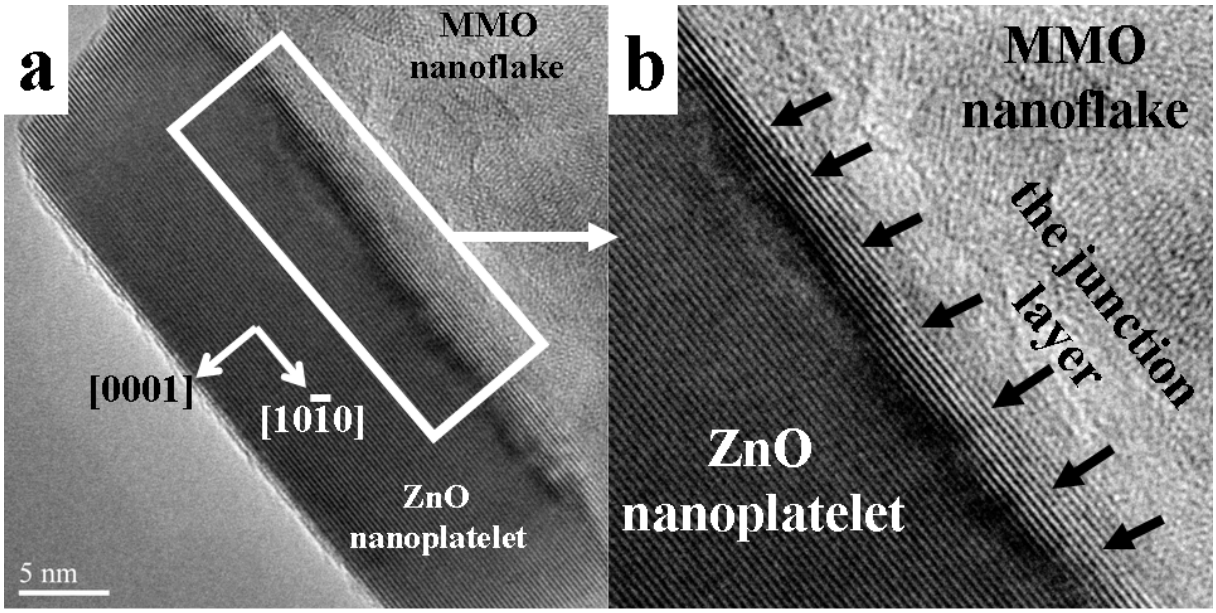

Fig. S5 HRTEM image of (a) the cross section of a ZnO nanoplatelet with exposed (0001) facet embedded on the F-MMO substrate; (b) magnification of the rectangular area in (a).

Nitrogen sorption:

The nitrogen adsorption–desorption isotherms and porosity of F-LDH and F-MMO are presented in Fig. S6. According to the BDDT classification, both the samples display a type IV isotherm with a type H3 hysteresis loop, implying the presence of mesopores. This was further confirmed by the corresponding pore-size distribution for which ranges of 2–5 nm for F-LDH and 2–25 nm for F-MMO were found (insets of Fig. S6). The Brunauer–Emmett–Teller (BET) surface areas of the F-LDH and F-MMO were calculated to be 62 and 84 m^2g^{-1}, respectively.

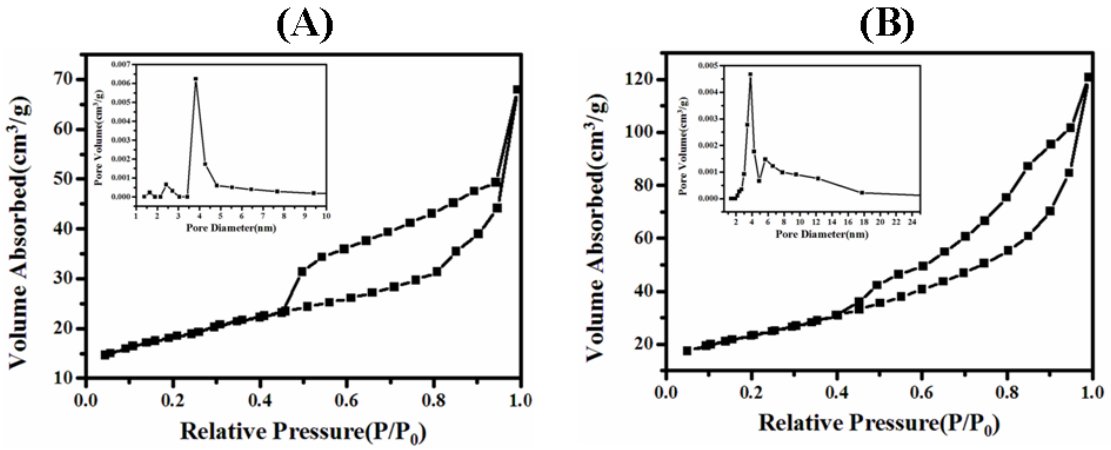

Fig. S6 Typical N_2 adsorption–desorption isotherms of (A) F-LDH and (B) F-MMO. Inset: the corresponding pore size distribution.

Evaluation of the photocatalytic activity:

To quantitatively evaluate the efficiency of photodegradation of RhB by the photocatalyst, the pseudo-first order model[11] was chosen:

$$\ln(C_0/C_t)=kt \qquad (1)$$

where C_0 and C_t are the concentrations of dye in solution at time 0 and t, respectively, and k is the pseudo-first order rate constant.

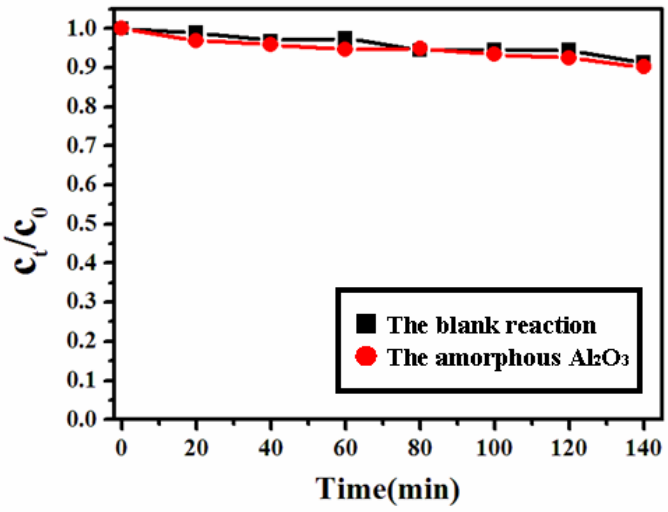

Fig. S7 Plots of the normalized concentration *vs.* irradiation time for the self-degradation (the blank reaction) and photodegradation of RhB by amorphous Al_2O_3 microspheres under visible light irradiation, respectively.

Table S1 Kinetic parameters for the photocatalytic decomposition of RhB by F-MMO, MMO powder, ZnO nanoplates and ZnO nanorods under visible light irradiation based on the pseudo-first order model

Photocatalyst	k_2 (min^{-1})	R^2
F-MMO	0.0175	0.9937
ZnAl-MMO	0.0078	0.9943
ZnO nanoplates	0.0062	0.9909
ZnO nanorods	0.0041	0.9976

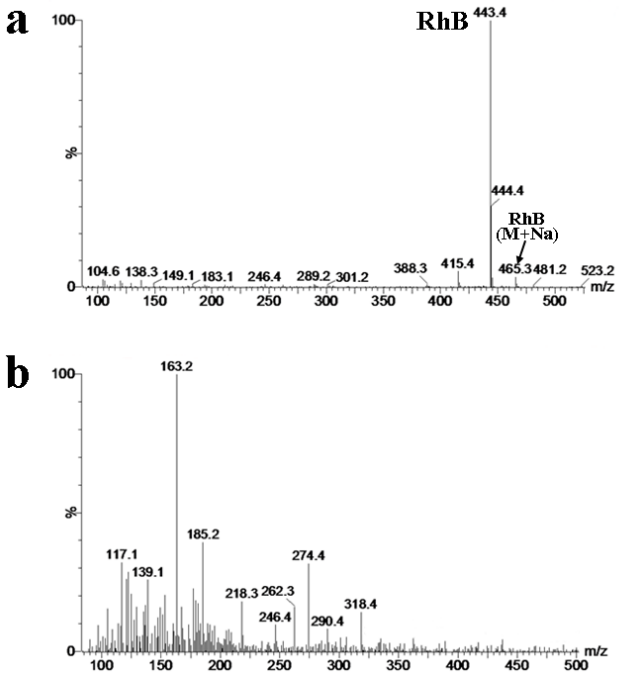

Fig. S8. Electrospray mass spectra recorded in the positive ion mode for (a) RhB solution; (b) photodecomposition products of RhB by F-MMO under visible light irradiation for 180 min.

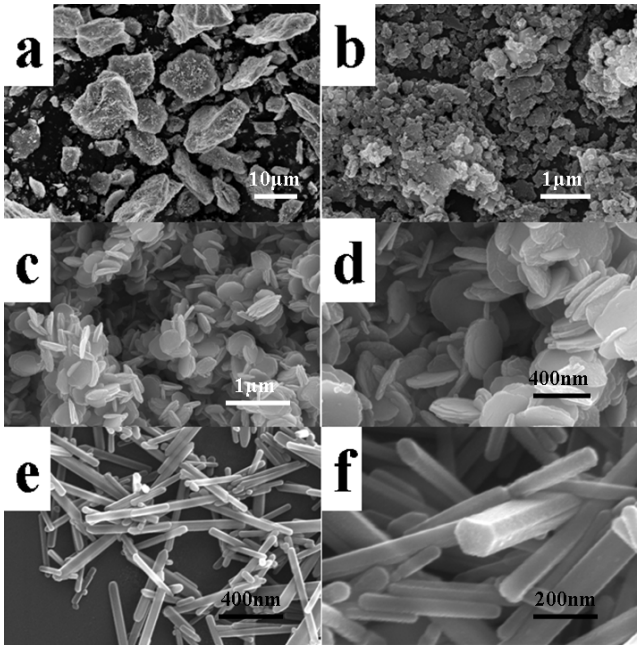

Fig. S9 SEM images at (a) low magnification and (b) high magnification of the ZnAl-MMO powder sample; (c) low magnification and (d) high magnification images of ZnO nanoplates; (e) low magnification and (f) high magnification images of ZnO nanorods.

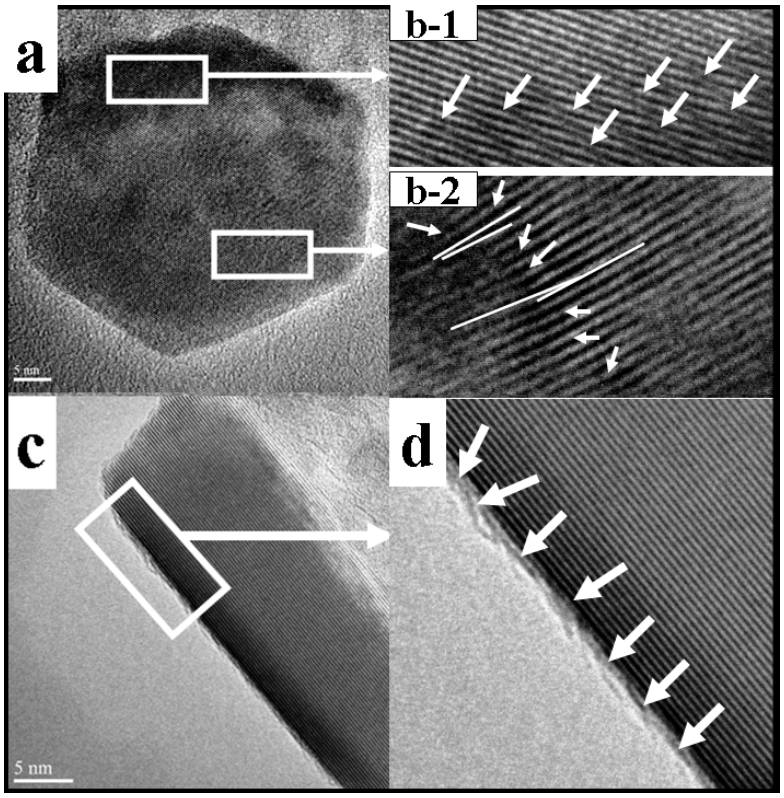

Fig. S10 HRTEM images of the F-MMO sample: (a) a single-crystalline ZnO nanoplatelet on the F-MMO substrate; (b-1) and (b-2) magnification of the rectangular area in (a); (c) the cross section of a ZnO nanoplatelet with exposed (0001) facet embedded on the F-MMO substrate; (d) magnification of the rectangular area in (c).

Details of the DFT calculations:

In order to give further insight into the visible light driven photocatalytic activity of the (0001) facets of ZnO, the total density of states (TDOS) as well as the local density of states (LDOS) for bulk ZnO, and the $(10\bar{1}0)$, (0001) and $(000\bar{1})$ surfaces, were calculated by density functional theory (DFT), with the purpose of illustrating the electronic structure of the crystal bulk state and the three surfaces based on their fully relaxed configurations. As shown in Fig. S11, the band gap of the (0001) Zn surface was calculated to be 1.3 eV, less than that of bulk ZnO (2.3 eV),

the $(10\bar{1}0)$ surface (1.8 eV) and the $(000\bar{1})$ surface (2.2 eV). The band gap value based on theoretical calculations is often underestimated due to the discontinuity of the exchange-correlation energy in DFT calculations with GGA functionals, but the trend for different surfaces is reliable.[12] The computational results further verify that the (0001) Zn facet is a highly-active surface which favors the electron–hole separation under visible light irradiation. Moreover, the DOS of these four structures are similar: the conduction band (CB) bottom is mainly constructed of Zn 4s4p states, and the valence band (VB) top primarily consists of O 2p and Zn 3d states. However, it is noteworthy that the VB top of the (0001) surface shifts in a more negative direction (as low as –0.80 eV), compared with that of bulk ZnO (0.50 eV), the $(10\bar{1}0)$ surface (0.70 eV) and the $(000\bar{1})$ surface (0.60 eV), indicating the strong oxidation potential of the (0001) Zn surface. The photocatalytic decomposition of organic compounds is known to require consumption of VB holes through the oxidation reaction. The strong oxidation potential of the (0001) surface will generate active holes, which can efficiently capture electrons from organic molecules and prevent recombination of holes and electrons. Therefore, the theoretical study shows that the ZnO nanoplatelets embedded on the F-MMO substrate with exposed (0001) facets possess both low band gap and low oxidation potential, accounting for the high visible light driven photocatalytic activity, in accordance with the experimental results.

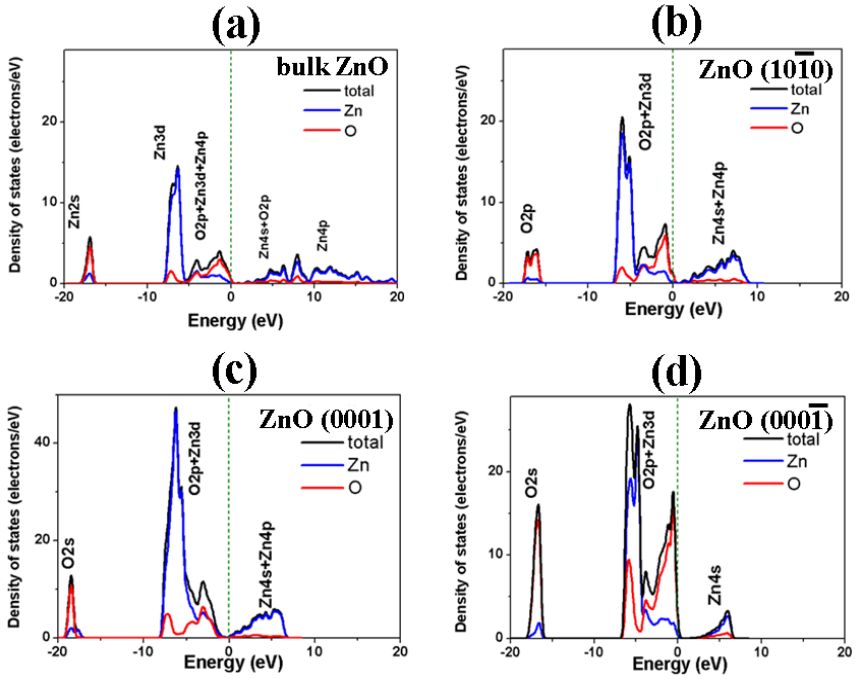

Fig. S11 Total and local electronic density of states (TDOS and LDOS) calculated for (a) bulk ZnO, (b) the relaxed ZnO(10$\bar{1}$0) surface, (c) the (0001) surface, and (d) the (000$\bar{1}$) surface.

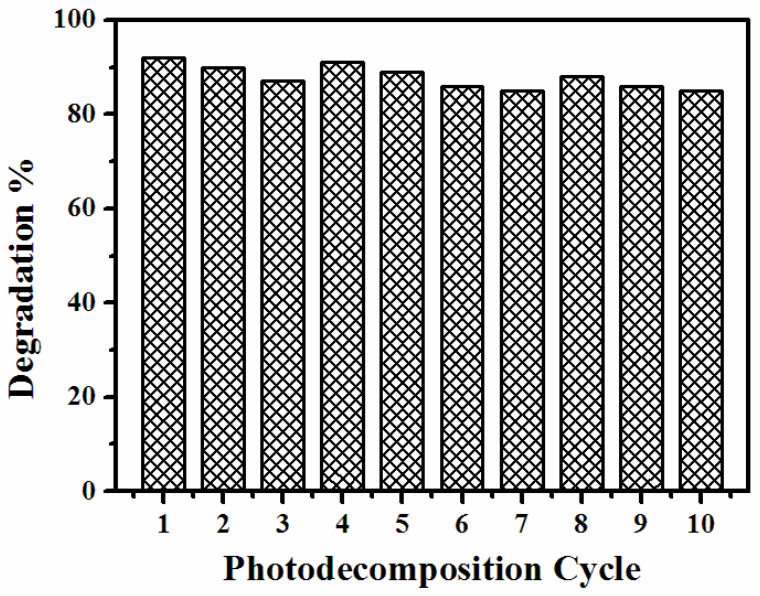

Fig. S12 Photocatalytic behavior of the F-MMO sample for the degradation of RhB over 10 consecutive cycles (the reaction time for each cycle was 140 min).

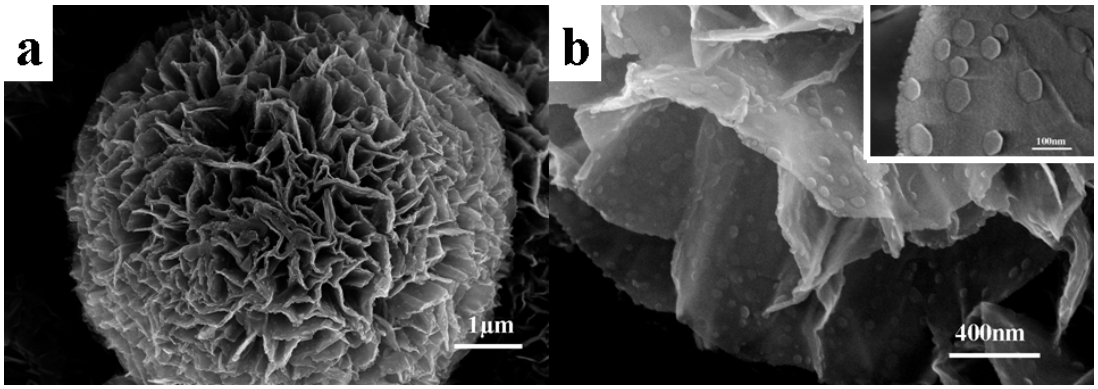

Fig. S13 SEM images of the F-MMO sample after 10 consecutive cycles of photocatalytic degradation of RhB: (a) low magnification, (b) high magnification.

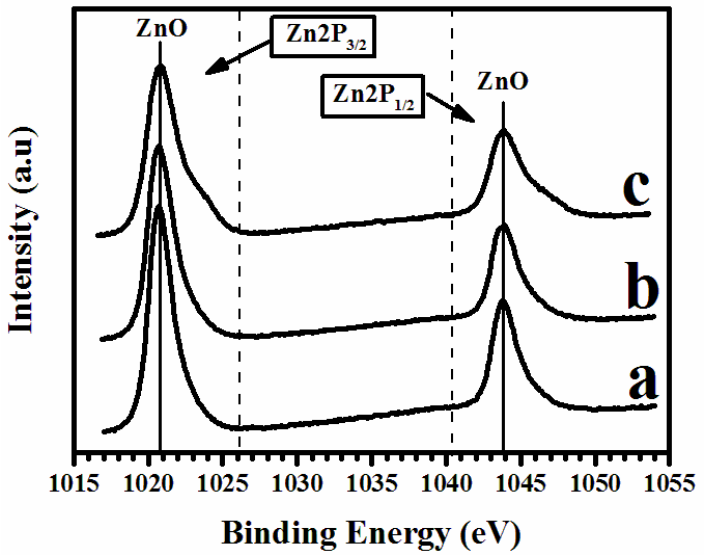

Fig. S14 Zn 2p XPS spectra of (a) the as-prepared F-MMO; (b) the F-MMO sample after the first cycle of photocatalytic degradation of RhB; (c) the F-MMO sample after 10 consecutive cycles of photocatalytic degradation of RhB.

References

1 W. Cai, J. Yu, B. Cheng, B. Su and M. Jaroniec, *J. Phys. Chem. C*, 2009, **113**, 14739.

2 H. Chen, F. Zhang, S. Fu and X. Duan, *Adv. Mater.*, 2006, **18**, 3089.

3 E. S. Jang, J. H. Won, S. J. Hwang and J. H. Choy, *Adv. Mater.*, 2006, **18**, 3309.

4 B. Cheng and E. T. Samulski , *Chem. Commun.*, 2004, **21**, 986.

5 C. Li and P. Choi, *J*. *Phys*. *Chem*. *C*, 2007, **111**, 1747.

6 C. Ruberto, Y. Yourdshahyan and B. I. Lundqvist, *Phys*. *Rev*. *B*, 2003, **67**, 195412.

7 M. D. Segall, P. J. D. Lindan, M. J. Probert, J. Pickard, P. J. Hasnip, S. J. Clark and M. C. Payne, *J*. *Phys*.: *Condens*. *Matter*, 2002, **14**, 2717.

8 J. A. White and D. M. Bird, *Phys*. *Rev*. *B*, 1990, **41**, 7892.

9 J. P. Perdew, K. Bruke and M. Ernzerhof, *Phys*. *Rev*. *Lett*., 1996, **77**, 3865.

10 D. Vanderbit, *Phys*. *Rev*. *B*, 1990, **41**, 7892.

11 J. M. Herrmann, H. Ahiri, Y. Ait-Ichou, G. Lassaletta, A. R. Gonzalez-Elipe and A. Fernandez, *Appl*. *Catal*. *B*, 1997, **13**, 219.

12 R. Asahi, Y. Taga, W. Mannstadt, A. Freeman, *J*. *Phys*. *Rev*. *B*, 2000, **61**, 7459.